Grain-boundary-limited transport in semiconducting SnO2 thin films: Model and experiments

Grain-boundary-limited transport in semiconducting SnO_2 thin films: Model and experiments

M. W. J. Prins,[a] K.-O. Grosse-Holz, J. F. M. Cillessen, and L. F. Feiner
Philips Research Laboratories, Prof. Holstlaan 4, 5656 AA Eindhoven, The Netherlands

(Received 28 July 1997; accepted for publication 6 October 1997)

We present a model that describes grain-boundary-limited conduction in polycrystalline semiconductors, for thermally assisted ballistic as well as diffusive transport, both for degenerate and nondegenerate doping. In addition to bulk parameters (the carrier effective mass and mean free path) the model contains grain boundary parameters (barrier height and width) and a coefficient of current nonuniformity. Temperature-dependent conductivity and Hall measurements on polycrystalline SnO_2 thin films with different Sb concentrations are consistently interpreted. © *1998 American Institute of Physics.* [S0021-8979(98)01302-4]

I. INTRODUCTION

Polycrystalline semiconductors find wide application in thin-film electronic and optoelectronic devices. Increasingly important are the high-mobility wide bandgap oxidic semiconductors (SnO_2,ZnO,In_2O_3, . . .) for transparent conducting electrodes,[1] for gas sensing devices,[2] and also as a channel material in thin-film transistors.[3] In the first case the material is degenerately doped, while for the other applications a nondegenerate semiconductor is required.

The electronic transport in polycrystalline semiconductors is often limited by scattering at the grain-boundary depletion layers. When the intergrain electrostatic barrier is larger than k_BT/e, the current can be described in terms of thermionic emission-diffusion of carriers across the grain boundaries (e.g., Refs. 4 and 5). However, thermionic emission theory is not applicable if the grain boundaries and interior of the grains can be degenerate as well as nondegenerate due to intentional and unintentional doping, as is, e.g., the case for polycrystalline oxidic semiconductors. The purpose of this article is to present a more general treatment of grain-boundary-limited conduction in polycrystalline semiconductors, that is applicable to thermally assisted ballistic as well as diffusive transport, for degenerate as well as nondegenerate doping. Our model depends on bulk parameters [the carrier effective mass and the mean free path (mfp)], grain boundary parameters (barrier height and width), and a coefficient of sample inhomogeneity. The model is applied to interpret temperature-dependent conductivity and Hall measurements on polycrystalline SnO_2 thin films with different Sb doping levels.

II. MODEL

In polycrystalline semiconductors the grain boundary scattering results from the electrostatic charge trapped at the intergrain boundaries, which sets up potential barriers to current flow. To describe the electronic properties of granular SnO_2 samples we separate the transport in the interior of the grains from the transport across the intergrain boundaries (for a review on this approach see Ref. 4). This separation is particularly useful if the mfp of the charge carriers is smaller than the grain size; this condition is satisfied for our experiments (see Secs. III and IV). We can distinguish three possibilities for the electron energy diagram of the grain interior and grain boundary (cf. Fig. 1). The barrier height Φ is defined as the energy difference between the Fermi level and the top of the barrier. Figure 1(a) applies to grains where the interior of the grains is degenerately doped and the top of the intergrain barrier is situated below the Fermi level ($\Phi<0$). Figure 1(b) corresponds to a degenerate grain interior with the top of the intergrain barrier above the Fermi level ($\Phi>0$). Finally, Fig. 1(c) represents the case of a nondegenerate semiconductor ($\Phi>0$). In the Appendix it is shown that for small voltages applied across the grain boundary ($e|V|<k_BT$), the barrier conductance g_b per unit area (units Ω^{-1} m^{-2}) is given by

$$g_b=\frac{4\pi e^2 m_e}{h^3}\frac{\ell}{\ell+\frac{3}{4}w}k_BT\ln\left[1+\exp\left(-\frac{\Phi}{k_BT}\right)\right], \qquad (1)$$

with the carrier mfp ℓ, the width of the barrier w, the electron charge e, the effective electron mass in the barrier m_e, and temperature T. Equation (1) was derived with the assumption that the electronic wavefunctions in the conduction band resemble free-electron states. Equation (1) covers the limit of thermally assisted ballistic transport ($\ell \gg w$) as well as the case of diffusive transport ($\ell \ll w$). The grain-boundary-limited conductivity of the sample equals

$$\sigma_b=\alpha_{\text{eff}}\,L g_b, \qquad (2)$$

where L is the average grain size. The coefficient α_{eff} ($0\leqslant\alpha_{\text{eff}}\leqslant 1$) takes account of the conductivity reduction due to a nonuniform current distribution. In an ideal sample consisting of equal-sized grains with intimate grain-to-grain contact and homogeneous barrier heights, the current would spread out evenly through the material. However, in general polycrystalline materials exhibit a considerable nonuniformity in grain size and presumably also in grain-boundary properties such as the barrier height. This results in an inhomogeneous distribution of the current, leading to a total cross-section for charge transport smaller than the sample cross-section.

[a]Correspondence to: Menno W. J. Prins, Philips Research Laboratories, Prof. Holstlaan 4, 5656 AA Eindhoven, The Netherlands; phone: +31.40.2742116; fax: +31.40.2743365 or 2743352; electronic mail: prins@natlab.research.philips.com

 0021-8979/98/83(2)/888/6/$15.00

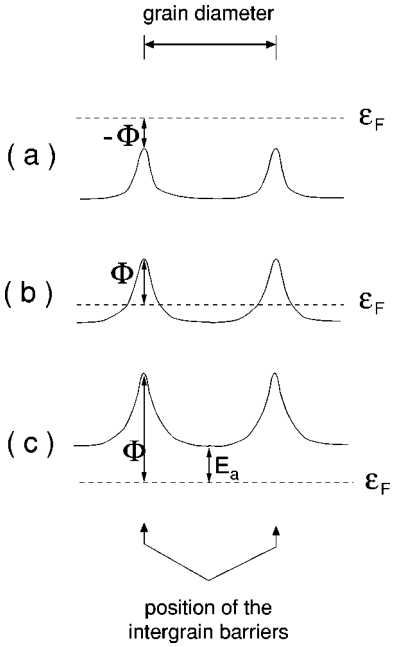

FIG. 1. One-dimensional conduction band diagram of a grain with intergrain barriers. Φ is the energy difference between the conduction band edge (solid lines) and the Fermi level (dashed lines) at the grain boundary. Panel (a): for a degenerate semiconductor with the Fermi level above the top of the barrier. Panel (b): for a degenerate semiconductor with the Fermi level below the intergrain electrostatic barrier. Panel (c): for a nondegenerate semiconductor, where E_a is the activation energy of carriers inside the grain.

In addition to measurements of conductivity, Hall effect measurements serve to further characterize the electronic properties of semiconductor materials. It is nontrivial to model the Hall constant for a granular material with an inhomogeneous current distribution. Nevertheless, if the grain size is larger than the carrier mfp ($L > \ell$), and the carriers outside the charge transporting filaments are assumed to be immobile, it can be shown that the measured carrier density n is a good approximation of the free carrier density inside the grains.[4] As we will find, the carrier density closely follows a behavior of thermal activation,

$$n \propto \exp(-E_a/k_B T), \tag{3}$$

where E_a is the activation energy of charge carriers $\{E_a = 0$ for a degenerately doped grain interior [Figs. 1(a) and 1(b)] and $E_a > 0$ for nondegenerate doping [Fig. 1(c)]$\}$. From the measured conductivity σ and the carrier density n derived from the Hall effect, it is customary to define an effective mobility μ^*,

$$\sigma \equiv ne\mu^* \Leftrightarrow \mu^* = \sigma/ne. \tag{4}$$

In case of grain-boundary-limited transport it is important to realize that the Hall effect yields an *effective* mobility: due to the electrostatic barriers, the free carrier density at the grain boundaries differs from the carrier density inside the grains. A repulsive electrostatic potential at the grain boundaries locally reduces the carrier density, hence the magnitude of the effective mobility is an *underestimate* of the true carrier mobility in the barrier region.

III. EXPERIMENTS

We have grown Sb-doped SnO_2 thin films by pulsed laser deposition utilizing the off-axis technique.[6] Five different SnO_2 targets were used, with an antimony concentration (N_{Sb}) ranging between 8 ppm (2×10^{17} cm^{-3}) and 13.5 $\times 10^3$ ppm (3.8×10^{20} cm^{-3}). The films were grown on ceramic Al_2O_3 substrates at a substrate temperature of 500 °C and in a 20 Pa O_2 ambient (more details on targets and preparation can be found in Ref. 7). Samples were grown with a film thickness between 100 and 300 nm. The sample thickness was measured with cross-sectional scanning electron microscopy to a precision of about 5%. Measurements by field-emission-gun scanning electron microscopy and scanning tunneling microscopy revealed that the films consist of grains with a diameter of 30–70 nm.[7] The granular structure is independent of the film thickness or the Sb concentration. X-ray diffraction and transmission electron microscopy data revealed that the films are polycrystalline without a preferred orientation and consist only of the SnO_2 phase. The sample conductivity has been determined with four-point van der Pauw measurements[8] using In contacts. Hall effect measurements were made in fields up to 10^6 A/m. For the samples with the lowest dopant concentration, we have observed a dependence of the electronic properties on the gaseous environment (e.g., the air humidity) due to the absence of a capping layer; at room temperature the observed changes are equivalent to a variation in the dopant concentration of about 10^{17}–10^{18} cm^{-3}.

IV. RESULTS AND DISCUSSION

Figure 2 shows the temperature dependence of the conductivity, carrier density, and effective mobility of SnO_2 thin films with different Sb concentrations (samples A–E, see Table I). At room temperature, we find a variation of conductivity by more than seven orders of magnitude, demonstrating the importance of doping for the conductivity. The samples of lowest dopant concentration show a nearly equal conductivity, indicating that the level of unintentional doping is reached. All samples exhibit a positive temperature dependence of the conductivity, indicative of a semiconductive behavior. The data of conductivity versus temperature are fitted to Eq. (2) of our model, where the barrier conductance is derived from Eq. (1). For each sample, the barrier height Φ and width w, the mfp ℓ, and the effective section α_{eff} are assumed to be independent of the temperature. The fitted parameters are given in Table I. Hall measurements yield n-type free carriers. Figure 2(b) shows the measured Hall carrier density and the fit to Eq. (3). For films with a charge carrier density $>10^{18}$ cm^{-3} we find a temperature-independent carrier density (degenerate semiconductor), while for lower carrier densities an activation energy up to 0.1 eV is measured; this behavior is in agreement with measurements on doped single-crystals.[9] The doping efficiency, n/N_{Sb}, ranges from the order of unity for heavy doping (A,B) to the order of 10^{-4} for low doping (D,E). This can be attributed to charge trapping in the intergrain states as well as to the nonnegligible thermal activation energy. The effective mobilities in Fig. 2(c) have been calculated from the

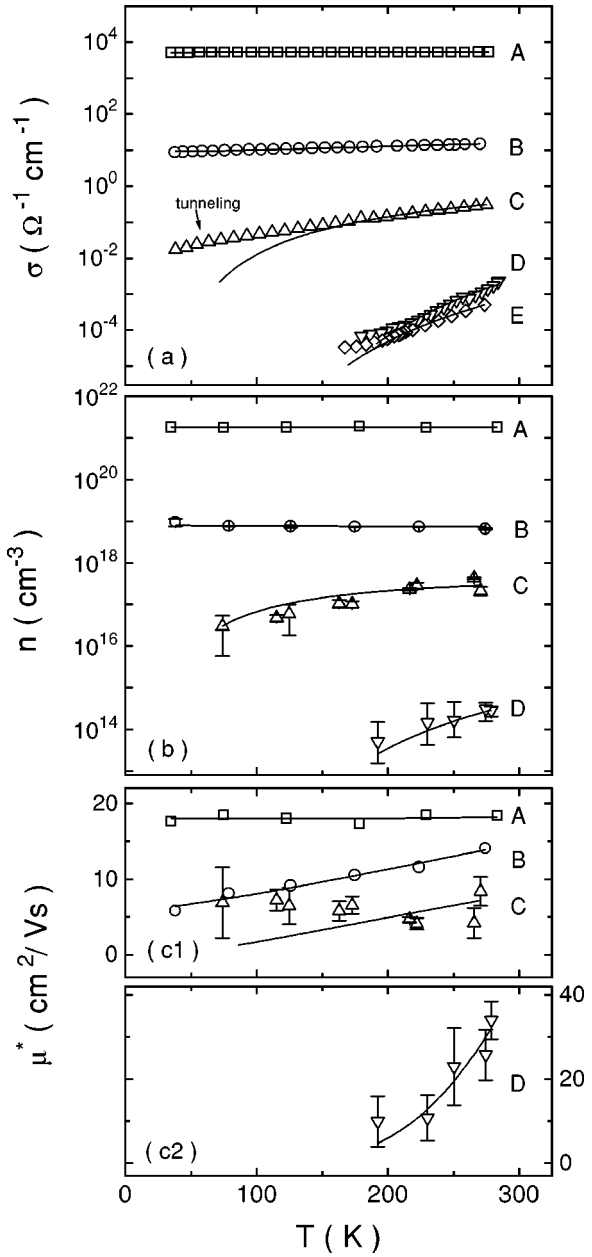

FIG. 2. (a) Conductivity, (b) carrier density, and (c) effective mobility of polycrystalline SnO_2:Sb thin films. Different symbols (squares, circles, ...) correspond to different dopant concentrations in the films (see Table I). In panels (a) and (b) the symbols represent measured data, while the lines are calculated with Eqs. (2) and (3), respectively. For the conductivity fit, the barrier height Φ, barrier width w, mfp ℓ, and effective section α_{eff} were assumed to be independent of temperature. The resulting fit parameters are given in Table I. The data and fits in panels (c1) and (c2) were calculated according to Eq. (4). For clarity the mobility data of sample D are plotted separately in panel (c2); note the difference in the scales of panels (c1) and (c2).

measured data and fitted curves by using Eq. (4). The mobilities are typically an order of magnitude lower than the values measured in single-crystalline samples of similar carrier density,[10,11] which already points to the importance of the grain boundaries in limiting the carrier transport. First, we will describe the results for the respective samples, mainly in terms of the energy band diagrams. Thereafter, we will discuss the prefactors deduced from the conductivity fits.

TABLE I. Results of conductivity fits [Eqs. (1) and (2)] and carrier density fits [Eq. (3)] as a function of temperature, for thin-film SnO_2 samples doped with Sb (dopant concentration N_{Sb}). The conductivity prefactor $\alpha_{\text{eff}} \cdot \ell/[\ell+(3/4)w]$ was calculated using $L=50$ nm and $m_e=0.2m_0$ (Ref. 9), both parameters having a relative uncertainty of a few tens of percents. The values between brackets represent the absolute fitting uncertainties.

		σ Fits		n Fits
Sample	N_{Sb} (cm^{-3})	Φ (meV)	$\alpha_{\text{eff}} \cdot \frac{\ell}{\ell+(3/4)w}$	E_a (meV)
A	3.8×10^{20}	<-70	...	0(2)
B	3.7×10^{19}	$-16(2)$	$3.7(0.4)\times10^{-2}$	0(5)
C	7.6×10^{18}	$+28(4)$	$2.9(0.4)\times10^{-3}$	20(8)
D	1.4×10^{18}	$+170(20)$	$5(2)\times10^{-3}$	90(60)
E	2×10^{17}	$+130(15)$	$4(2)\times10^{-4}$	...

The sample of highest dopant concentration (A) shows a negligible temperature dependence of the conductivity ($<3\%$ variation over a temperature range of nearly 300 K) and the carrier density. This implies that at the grain boundaries the Fermi level is situated well above the conduction band minimum [Fig. 1(a)]: due to the high dopant concentration the electrostatic barriers at the grain boundaries are negligible. Also the interior of the grains is degenerately doped, as is evidenced by the temperature-independence of the carrier density. The temperature-independent transport exhibits a mobility of 18 cm^2/Vs. The carrier scattering can be attributed to scattering at neutralized grain boundary states and scattering in the dopant impurity band.

Sample B shows a temperature-dependence of the conductivity that corresponds to a barrier height of -16 meV, while the interior of the grains is degenerate [situation of Fig. 1(b)]. Using the measured carrier density, we can estimate the energy difference between the Fermi level and the conduction band minimum inside the grains to be 70 ± 30 meV (Ref. 12). This is much larger than k_BT, in agreement with the measured temperature-independence of the carrier density. The positive temperature dependence of the effective mobility results from the non-negligible barrier at the grain boundaries.

Sample C exhibits a moderate temperature dependence of the conductivity. The model underestimates the conductance at low temperatures; this could be due to tunneling through the intergrain barriers, which has not been included in the derivation of Eq. (1). The moderate temperature-dependence of the carrier density indicates that the material is in an intermediate situation between a degenerate and a nondegenerate semiconductor. The calculated mobility curve shows some deviations from the measured data, which is a direct consequence of the imperfect model of the conductivity.

Sample D shows a very strong temperature-dependence of the conductivity and a less strong temperature-dependence of the carrier density. This situation corresponds to the band diagram of Fig. 1(c). Due to the intergrain barrier ($\Phi>E_a$) the effective carrier mobility shows a strong positive temperature-dependence, which contrasts to the negative temperature dependence of high-purity single-crystals.[10] As a result of the electrostatic barriers, the measured mobility is

an underestimate of the intrinsic SnO_2 conduction band mobility [cf. Eq. (4)]. In spite of a difference in antimony concentration, the electronic properties of sample E and sample D are quite similar, indicating that the level of unintentional doping is reached. The temperature-dependence of the carrier density and mobility of sample E is not shown due to the large measurement uncertainties.

The prefactors $\alpha_{\mathrm{eff}} \cdot \ell/[\ell+(3/4)w]$ that follow from the conductivity fits are listed in Table I (the factor could not be determined for sample A due to the weak temperature dependence). Parameter α_{eff} takes account of the reduced transport section; the fraction $\ell/[\ell+(3/4)w]$ equals unity for ballistic transport ($\ell \gg w$) and $4\ell/3w$ for diffusive transport ($\ell \ll w$). The mfp ℓ can be estimated to be 7 nm for single-crystalline SnO_2 at room temperature,[13] and 4 nm for degenerately doped SnO_2.[14] In sample B the width of the electrostatic barrier is about 3 nm (twice the Fermi wavelength); since this is similar to the mfp, we can conclude that carrier transport across the barriers is closely ballistic. Hence, in this sample the prefactor is a good estimation of the effective transport section α_{eff} in this sample, being of the order of 10^{-2}. These results indicate that only a fraction of the sample is efficiently guiding the current. As was stated with Eq. (2), we attribute the reduction of the transport section to the granular nature and inhomogeneity of the sample, i.e., variations in barrier height and in grain size.

The prefactor tends to decrease for samples of lower doping density. This can be attributed to an increase of the barrier width for samples of lower dopant concentration. The maximum barrier width is about 40 nm (Ref. 15) (roughly the average grain size); assuming a minimum mfp of 2 nm, we estimate a lower limit of ℓ/w to be about 2/40 nm $=5\times10^{-2}$. We conclude that the numerical value of the prefactor of the conductivity equation is given by an effective transport section of the order of 10^{-2}, with an additional reduction by one or two orders of magnitude in nondegenerate samples due to the diffusive nature of the transport.

V. SUMMARY AND CONCLUSIONS

We have discussed conductivity and Hall data of polycrystalline SnO_2:Sb thin films in terms of a grain-boundary-limited transport model. The carrier density of the films spans a wide range (10^{14}–10^{21} cm^{-3}), controlled by the dopant concentration. The temperature-dependence of the carrier concentration is similar to what is observed in single crystals (activation energy between zero and 0.1 eV). However, the conductivity of all films shows a positive temperature-dependence and is significantly lower than in single-crystals. For this behavior we have provided a consistent explanation with our model, which includes scattering at the grain-boundary barriers and a coefficient of nonuniform charge flow through the sample (effective transport section). For a carrier density below 10^{18} cm^{-3} the material is nondegenerate and the conductivity is limited by carrier diffusion (instead of by ballistic emission) across the grain boundary barriers; due to the intergrain repulsive potential the carrier mobility depends strongly on the temperature. At higher dopant concentrations the interior of the grains becomes degenerate; the conductivity is limited by ballistic transport across the barriers, which can be temperature dependent if the Fermi level is not situated sufficiently above the conduction band in the intergrain region. The effective transport section is estimated to be of the order of 10^{-2}; this is attributed to a nonuniform current distribution, caused by inhomogeneities in grain size and barrier height. For future work it will be interesting to include tunneling in the transport model (see, e.g., Ref. 16), and to quantify the effective transport section by simulating the charge transport in an inhomogeneous granular film. Finally, it will be interesting to explore the significance of this grain-boundary-limited transport model for other polycrystalline materials, such as for gas-sensing oxidic systems.

ACKNOWLEDGMENTS

The authors thank P. W. M. Blom and M. J. M. de Jong for in-depth discussions and for critically reading the manuscript.

APPENDIX: BARRIER CONDUCTANCE

In this Appendix we derive an equation for the conductance of a planar electrostatic barrier separating two reservoirs (i.e., two grains). The equation is derived with the transmission approach (Landauer formalism) and applies for ballistic transport (when the carrier mfp is larger than the barrier width) as well as diffusive transport (when the mfp is smaller than the barrier width). As an additional exercise, we show that in the diffusive limit the same equation for the conductance can be derived with the Drude formalism.

a. Landauer formalism: Ballistic and diffusive transport. The influence of elastic scattering on the current is described by the two-terminal Landauer equation (for a review see Ref. 17),

$$J=\frac{1}{A}\frac{2e}{h}\int_{-\infty}^{\infty} d\epsilon[f_1(\epsilon)-f_2(\epsilon)]\mathrm{Tr}\; t(\epsilon)t^{\dagger}(\epsilon), \tag{A1}$$

where J is the current density across the barrier, A is the cross-sectional area of carrier transport, e is the electron charge, h is Planck's constant, f_1 and f_2 are the Fermi distribution functions in the reservoirs, and $t(\epsilon)$ is the matrix of transmission probability amplitudes of states at energy ϵ. Calculation of the transmission matrix $t(\epsilon)$ requires knowledge of the electrostatic barrier profile and the electron wavefunctions. Let us assume that the states inside the barrier can be described by free-electron wavefunctions with an effective mass m_e, having an energy offset Φ with respect to the Fermi level (situated at $\epsilon=0$). For a channel with a two-dimensional cross-section, the number of transmission modes at energy ϵ equals

$$N(\epsilon)=\begin{cases}\dfrac{Ak^2}{4\pi}=\dfrac{A}{4\pi}\dfrac{2m_e}{\hbar^2}(\epsilon-\Phi) & \text{if} \quad \epsilon>\Phi \\ 0 \quad \text{otherwise.}\end{cases} \tag{A2}$$

Here we neglect quantization effects in the barrier region[18] and use the semiclassical expression.[17] If we assume a unity

transmission probability for these free-electron states, it can be shown that the transmission trace to a good approximation equals[19]

$$\mathrm{Tr}\ t(\epsilon)t^{\dagger}(\epsilon)=N(\epsilon)\left[1+\frac{3}{4}\frac{w}{\ell(\epsilon)}\right]^{-1}, \tag{A3}$$

where $\ell(\epsilon)$ is the carrier mfp and w the width of the barrier. For a voltage drop across the barrier smaller than k_BT [linear response (Ref. 20)] the following applies:

$$f_1(\epsilon)-f_2(\epsilon)=-eV\frac{\partial f}{\partial \epsilon}. \tag{A4}$$

Neglecting the transmission of electrons with an energy lower than Φ (no electron tunneling) and assuming an energy-independent mfp, we find from Eqs. (A1)–(A4) the following expression for the barrier conductance per unit area,

$$g=\frac{J}{V}=\frac{2e^2}{h}\frac{2m_e}{4\pi\hbar^2}\frac{\ell}{\ell+(3/4)w}\int_{\Phi}^{\infty}d\epsilon(\epsilon-\Phi)\left(-\frac{\partial f}{\partial \epsilon}\right)$$

$$=\frac{2e^2}{h}\frac{m_e}{2\pi\hbar^2}\frac{\ell}{\ell+(3/4)w}k_BT\ \ln\left[1+\exp\left(-\frac{\Phi}{k_BT}\right)\right]. \tag{A5}$$

This equation describes the barrier conductance due to thermally assisted ballistic as well as diffusive transport, for arbitrary value of the barrier height (note the usage of h as well as $\hbar$ in the formulas). In case $\Phi \gg k_BT$ we recover

$$g=\frac{4\pi e^2 m_e}{h^3}\frac{\ell}{\ell+(3/4)w}k_BT\ \exp\left(-\frac{\Phi}{k_BT}\right). \tag{A6}$$

For $\ell \gg w$ this equals the well-known equation for thermionic emission[21] at small applied voltage ($e|V| \ll k_BT$). For a negative barrier height with $\Phi \ll -k_BT$, Eq. (A5) becomes

$$g=\frac{2e^2}{h}\frac{m_e}{2\pi\hbar^2}\frac{\ell}{\ell+(3/4)w}|\Phi|, \quad \text{for} \quad \Phi \ll -k_BT, \tag{A7}$$

which equals the conductance of a ballistic point contact.[17,19]

b. Drude formalism: Diffusion only. In case the barrier conductance is limited by scattering inside the barrier, the current density can be approximated by

$$J=en_bv_d, \tag{A8}$$

where n_b is the free-carrier density in the barrier region, and v_d is the diffusion velocity. Assuming free-electron wavefunctions inside the barrier, the free-carrier density is given by[21]

$$n_b=N_c\frac{2}{\sqrt{\pi}}F_{1/2}\left(-\frac{\Phi}{k_BT}\right),$$

$$\text{with} \quad N_c=2\left(\frac{2\pi m_e k_BT}{h^2}\right)^{3/2}, \tag{A9}$$

where N_c is the effective conduction band density of states inside the barrier, and $F_{1/2}$ is the Fermi–Dirac integral.[21] The diffusion velocity is given by $v_d=\mu_bE$, where μ_b and E are the carrier mobility and electrostatic field in the barrier, respectively. The field is $\sim V/w$, where w is the width of the barrier. This yields for the barrier conductance in the diffusive limit

$$g_{\mathrm{diff}}=J/V=\frac{e\mu_b}{w}N_c\frac{2}{\sqrt{\pi}}F_{1/2}\left(-\frac{\Phi}{k_BT}\right). \tag{A10}$$

The carrier mobility in the barrier can be expressed in terms of the carrier relaxation time τ or the carrier mfp ℓ,

$$\mu_b=\frac{e\tau}{m_e}=\frac{e\ell}{\overline{c}\,m_e}, \tag{A11}$$

where $\overline{c}$ is the average carrier velocity. In case $\Phi \gg k_BT$, the kinetic energy of free carriers ($m_e\overline{c^2}/2$) equals $(3/2)k_BT$. It is easily shown that in this limit Eq. (A10) becomes

$$g_{\mathrm{diff}}=\frac{4\pi e^2 m_e}{h^3}\frac{\ell}{w}\sqrt{\frac{2\pi}{3}}k_BT\ \exp\left(-\frac{\Phi}{k_BT}\right), \tag{A12}$$

which nearly reproduces Eq. (A6) in the diffusive limit ($\ell \ll w$). Similarly, it can be shown that for $\Phi \ll -k_BT$ (when the average carrier velocity is given by the Fermi velocity) Eq. (A10) is in agreement with Eq. (A7).

[1] K. L. Chopra, S. Mayor, and K. Pandya, Thin Solid Films **102**, 1 (1983).
[2] See, e.g., W. Göpel and K. D. Schierbaum, Sens. Actuators B **26–27**, 1 (1995).
[3] M. W. J. Prins, J. F. M. Cillessen, J. B. Giesbers, and S. E. Zinnemers, Appl. Phys. Lett. **70**, 458 (1997).
[4] J. W. Orton and M. J. Powell, Rep. Prog. Phys. **43**, 1263 (1980).
[5] P. V. Evans and S. F. Nelson, J. Appl. Phys. **69**, 3605 (1991).
[6] N. J. Ianno and K. B. Erington, Rev. Sci. Instrum. **63**, 3525 (1992); J. F. M. Cillessen, M. J. M. de Jong, and X. Croisé, Rev. Sci. Instrum. **67**, 3229 (1996).
[7] K.-O. Grosse-Holz, J. F. M. Cillessen, M. W. J. Prins, P. W. M. Blom, R. M. Wolf, L. F. Feiner, and R. Waser, Mater. Res. Soc. Symp. Proc. **401**, 67 (1996).
[8] L. J. van der Pauw, Philips Res. Rep. **13**, 1 (1958); A. A. Ramadan, R. D. Gould, and A. Ashour, Thin Solid Films **239**, 272 (1994).
[9] Z. M. Jarzebski and J. P. Marton, J. Electrochem. Soc. **123**, 299C (1976).
[10] C. G. Fonstad and R. H. Rediker, J. Appl. Phys. **42**, 2911 (1971).
[11] J. A. Marley and R. C. Dockerty, Phys. Rev. **140**, A304 (1965).
[12] In a free-electron model the Fermi energy is given by: $\epsilon_F=\hbar^2/2m_e(3\pi^2n)^{2/3}$. For $n=7.5\times10^{18}$ cm^{-3} (sample B) and $m_e=0.2(0.1)m_0$ (Ref. 9) one has $\epsilon_F=70(30)$ meV.
[13] The carrier mfp ℓ is given by: $\ell=\mu\overline{c}\,m_e/e$, where μ is the carrier mobility and $\overline{c}$ is the carrier velocity. In a nondegenerate semiconductor the kinetic energy of free carriers equals $(3/2)k_BT$, such that $\overline{c}\simeq(3k_BT/m_e)^{1/2}$. Thus $\ell=\mu\overline{c}\,m_e/e\simeq(3k_BTm_e)^{1/2}\mu/e$. In SnO_2 single-crystals, the room-temperature carrier mobility is about 250 cm^2/Vs (Ref. 10); with $m_e=0.2(0.1)m_0$ (Ref. 9) we find ℓ = 7.3(1.8) nm.
[14] For a degenerately doped semiconductor with free-electron bandstructure the carrier velocity equals the Fermi velocity: $v_F=(\hbar/m_e)(3\pi^2n)^{1/3}$, such that $\ell=\hbar(3\pi^2n)^{1/3}\mu/e$. In the limit of very high doping of a polycrystalline semiconductor, the electrostatic barriers at the grain boundaries are negligible and the carrier mobility is limited by neutral impurity scattering. Now using the measured data of sample A ($n=1.8\times10^{21}$ cm^{-3} and $\mu=18$ cm^2/Vs) we find ℓ = 4.4 nm.
[15] In the depletion approximation the Schottky barrier width equals $(2\epsilon_0\epsilon_rV_{bb}/eN)^{1/2}$, where V_{bb} is the band-bending voltage (Ref. 21). Using $\epsilon_r=10$, $V_{bb}\simeq0.1$ V, and $N=2\times10^{17}$ cm^{-3}, we find a depletion width of about 20 nm. The intergrain barrier consists of two back-to-back Schottky barriers, such that the total width of the depleted region is about 40 nm.
[16] G. D. Mahan, L. M. Levinson, and H. R. Philipp, J. Appl. Phys. **50**, 2799 (1979).

[17] C. W. J. Beenakker and H. van Houten, Solid State Phys. **44**, 1 (1991).
[18] The importance of quantum interference in the barrier can be estimated as follows: The maximum spacing of energy levels is given by $(\hbar^2/2m_e) \times(\pi/L)^2$, where L is a typical length scale of the system. For our experiments L is the diameter of the SnO_2 grains (30–70 nm) which gives a maximum energy-level spacing of about 1 meV. This plays no role at our measuring temperatures, for which k_BT is larger than 3 meV.
[19] M. J. M. de Jong, Phys. Rev. B **49**, 7778 (1994).
[20] Nonlinearities are expected when the voltage drop per grain boundary exceeds k_BT/e. In our samples the average grain diameter is 50 nm, while the sample size is a few millimeters. Hence, we expect nonlinearities for applied voltages larger than $2\times10^4\ k_BT/e$, which at 100 K equals a few hundred volts, nearly two orders of magnitude larger than the voltages we apply.
[21] S. M. Sze, *Physics of Semiconductor Devices* (Wiley, New York, 1981).